Results in Physics 8 (2018) 213–222

Contents lists available at ScienceDirect

Results in Physics

journal homepage: www.journals.elsevier.com/results-in-physics

Multiple slips effects on MHD SA-Al_2O_3 and SA-Cu non-Newtonian nanofluids flow over a stretching cylinder in porous medium with radiation and chemical reaction

I. Tlili [a,*], W.A. Khan [a], I. Khan [b]

[a] Department of Mechanical and Industrial Engineering, College of Engineering, Majmaah University, Majmaah 11952, Saudi Arabia
[b] Department of Basic Sciences, College of Engineering, Majmaah University, Majmaah 11952, Saudi Arabia

ARTICLE INFO

Article history:
Received 25 October 2017
Received in revised form 28 November 2017
Accepted 6 December 2017
Available online 9 December 2017

Keywords:
SA-NaAlg-based non-Newtonian nanofluid
SWNCTs and MWCNTs
Thermal radiation
Chemical reaction
MHD and porosity
Multiple slips

ABSTRACT

The purpose of this communication is to examine the collective influence of velocity, and thermal slips on magnetohydrodyanmics (MHD) SA-Al_2O_3 and SA-Cu non-Newtonian nanofluids flow over a stretching cylinder in porous medium together with thermal radiation and chemical reaction effects. Sodium Alginate (SA-NaAlg) is taken as non-Newtonian base fluid. Two types of nanoparticles alumina or aluminum oxide (Al_2O_3) and copper (Cu) are suspended in sodium alginate (SA) which is taken as base fluid, an example of non-Newtonian Casson fluid. The formulated nonlinear partial differential equations with auxiliary boundary conditions are transformed into non-dimensional form by applying suitable similarity transformations. The resulting dimensionless problem is solved numerically using shooting and fourth order Runge-Kutta method. The impacts of various thermophysical parameters on local skin-friction, local Nusselt number, temperature and velocity are analyzed through graphs as well as in tabular form and discussed in detail. A comparison between SA-Al_2O_3 and SA-Cu nanofluids is clearly shown and in limiting sense the present results are compared with published results from literature. The results show that with magnetic parameter, skin-friction and Nusselt number both decreased, and Nusselt numbers are the highest in case of Al_2O_3 than Cu nanoparticles.

© 2017 The Authors. Published by Elsevier B.V. This is an open access article under the CC BY-NC-ND license (http://creativecommons.org/licenses/by-nc-nd/4.0/).

Introduction

Several biological and industrial fluids such as ceramics, polymers, liquid detergents, lubricating greases, multi-grade oils, gypsum pastes, printer inks, blood, paints and fruit juices do not obey the classical Newton's law of viscosity. Such liquids continuously change their viscosities under the shear stress and are known as non-Newtonian fluids. Since all non-Newtonian fluids have different physical and thermal properties, therefore, it was not possible to describe them all by using a single constitutive relation same like Newtonian fluids [1,2], hence several non-Newtonian fluid models have been developed in the literature. Each non-Newtonian fluid model has its own importance and deficiencies. For example, Maxwell model is considered as one of the simplest rate type fluid models which has the tendency to predict the effects of fluid relaxation time [3]. Second grade fluid is the simplest model in differential type fluids, which has both viscous and elastic effects [4]. Power-law model can describe shear-thinning and shear-thickening behavior, but cannot explain the normal stress differences in the flow [5].

In fact, for (MHD) flow over stretching surface in the presence of thermal radiation and magnetic field with heat generation/absorption have been addressed by Hayat [6], they found that skin friction coefficient improves melting parameter and the concentration decrease with Schmidt number. This study in [6] was further extended in [7] to include moving stretching sheet characterized by it is adaptable thickness, the results reveled clear enhancement on velocity for in increment of Reynolds number while temperature lessen heat transfer rate. Recently some investigation dealing with magnetohydrodynamics (MHD) flow and heat transfer analysis for different type of micropolar nanofluid like Jeffrey, Walter-B, thixotropic nanofluid over stretching sheet or cylinder have been explored numerically [8–12] showing the behaviors and the effect of pertinent physical parameters on the skin friction coefficient and Nusselt number (Tables 1–4).

Apart from the above and many other fluid models, there is one known as Casson fluid model, introduced by Casson in 1959 [13]. This model is a preferred rheological model for many fluids including blood, tomato sauce, honey, soup, orange juice and chocolate.

* Corresponding author.
E-mail address: l.tlili@mu.edu.sa (I. Tlili).

https://doi.org/10.1016/j.rinp.2017.12.013
2211-3797/© 2017 The Authors. Published by Elsevier B.V.
This is an open access article under the CC BY-NC-ND license (http://creativecommons.org/licenses/by-nc-nd/4.0/).

Table 1
Comparison of skin friction $-f''(1)$ for several values of Re_D when $\beta \to \infty$ and $M = Q_0 = Nr = 0$, $\phi = Ec = \gamma = \lambda = t = s = 0$.

Re_D	Ishak et al. [2]	Wang [1]	Present
0.5	0.8827	0.8822	0.8959
1	1.1781	1.1777	1.1833
2	1.5941	1.5939	1.5958
5	2.4175	2.4174	2.4177
10	3.3445	3.3444	3.3445

Table 2
Comparison of Nusselt number $-\theta'(1)$ for several values of Pr when $Re_D = 10, \beta \to \infty$ and $M = Q_0 = Nr = 0$, $\phi = Ec = \gamma = \lambda = t = s = 0$.

Pr	Ishak et al. [2]	Wang [1]	Present
2	3.036	3.035	3.0359
7	6.1592	6.16	6.1580
10	7.4668	10.77	7.4644

Table 3
Comparison of skin friction $-f''(1)$ for different values of solid volume fraction of different nanoparticles when $Re_D = 1, M = 5, \beta \to \infty$ and $Q_0 = Nr = 0$, $Ec = \gamma = \lambda = t = s = 0$.

ϕ	Ashorynejad et al. [33]		Present results	
	Cu	Al_2O_3	Cu	Al_2O_3
0.05	2.6025	2.5571	2.6025	2.5570
0.1	2.5131	2.4300	2.5130	2.4299
0.15	2.4147	2.3011	2.4147	2.3010
0.2	2.3083	2.1706	2.3082	2.1705

Table 4
Comparison of skin friction $-f''(1)$ for different values of magnetic field when $Re_D = 1, \phi = 0.1, \beta \to \infty$ and $Q_0 = Nr = 0$, $Ec = \gamma = \lambda = t = s = 0$.

M	Ashorynejad et al. [33]		Present results	
	Cu	Al_2O_3	Cu	Al_2O_3
0	1.3734	1.2057	1.3570	1.1821
1	1.6744	1.5418	1.6710	1.5374
5	2.5131	2.4300	2.5130	2.4299
10	3.2456	3.1828	3.2456	3.1828

Table 5
Comparison of Nusselt number $-\theta'(1)$ for different values of magnetic field when $Re_D = 1, Pr = 6.2, \phi = 0.1, \beta \to \infty$ and $Q_0 = Nr = 0$, $Ec = \gamma = \lambda = t = s = 0$.

M	Ashorynejad et al. [33]		Present results	
	Cu	Al_2O_3	Cu	Al_2O_3
0	3.0106	3.0945	3.8630	3.2897
1	2.8745	2.9414	3.6464	3.1642
5	2.5325	2.5705	3.1341	2.8453
10	2.2993	2.3244	2.7563	2.5829

This model exhibits a yield stress. Casson fluid behaves as solid when the shear stress is less than the yield stress and it starts to deform when shear stress becomes greater than the yield stress. Some recent studies concerning the flow and heat transfer analysis of regular Casson fluid can be found in Refs. [14–24]. However, in all these studies, Casson fluid was considered as a regular fluid with quite low thermal conductivity, which is not of enough benefit for many enhanced heat transfer processes in industry. A New numerical method is developed by Abou-zeid [25] using the homotopy perturbation method to examine the flow of micropolar non-Newtonian nanofluid characterized by it is incompressibility and peristaltic motion, the results shown that the nanoparticles

Table 6
Comparison of Nusselt number $-\theta'(1)$ for different values of solid volume fraction of different nanoparticles when $Re_D = 1, Pr = 6.2, M = 5, \beta \to \infty$ and $Q_0 = Nr = 0$, $Ec = \gamma = \lambda = t = s = 0$.

ϕ	Ashorynejad et al. [33]		Present results	
	Cu	Al_2O_3	Cu	Al_2O_3
0.05	2.8239	2.8462	3.3899	2.9973
0.1	2.5325	2.5705	3.6836	2.8453
0.15	2.2797	2.3280	4.0362	2.6760
0.2	2.0584	2.1128	4.4811	2.4881

Table 7
Comparison of Nusselt number $-\theta'(1)$ for regular fluid (Sodium Alginate) and $Re_D = 10, \beta \to \infty$ $M = \phi = Q_0 = Nr = Ec = \gamma = \lambda = t = s = 0$.

Pr	Wang [1]	Ishak et al. [2]	Ahmed et al. [31]	Pandey and Kumar [32]	Present results
2	3.035	3.0360	3.03553	3.03534	3.03593
7	6.160	6.1592	6.15776	6.15590	6.15798
10	10.77	7.4668	7.46419	7.46230	7.46438

phenomena has an opposite comportment regarding the temperature profile. El-dabe et al. [26] studied numerically the peristaltic motion of a non-Newtonian nanofluid in the presence of magnetic field, thermal radiation with heat generation and viscous dissipation, they approve the same results found in [25] and demonstrate that the axial velocity increases with magnetic field and Brownian motion. Numerical methods used to investigate non Newtonian nanofluid flow and heat transfer with Peristalsis and the effect of gliding motion of bacteria to explore the velocity and temperature profiles and nanoparticles behaviors [27–29].

Choi [30], in 1995, for the first time realized that the thermal conductivity of regular working fluids can be enhanced by dispersing nanometer-sized materials (between 1 and 100 nm), can be in the form of nanoparticles, nanofibers, nanotubes, nanowires, nanorods, nanosheet, or droplets. This mixture of base fluid and nanometer-sized materials is called nanofluid. Nanofluids have been initiated to acquire the improved thermo physical properties such as thermal conductivity, thermal diffusivity, viscosity, and convective heat transfer coefficients which were compared to those of base fluids like oil or water [31–35]. Thermal properties of nanofluids very much depend on size, shape, as well as volume fraction of nanoparticles in the base fluid and the base fluid itself. Base on the great impending applications of nanofluids in many fields, investigators from different areas contributed in the field of nanofluids either theoretically of experimentally. However, we focus here on the investigations related to Casson nanofluids.

Haq et al. [36] studied convective heat transfer and MHD effects on Casson nanofluid flow over a shrinking sheet. Nadeem et al. [37] examined MHD three-dimensional boundary layer flow of Casson nanofluid past a linearly stretching sheet with convective boundary condition. Abolbashari et al. [38] examined entropy generation for Casson nanofluid flow induced by a stretching surface. Hussain et al. [39] studied Casson nanofluid flow with viscous dissipation and convective conditions. Sulochana et al. [40] established similarity solution of 3D Casson nanofluid flow over a stretching sheet with convective boundary conditions. Ibukun et al. [41] presented the unsteady Casson nanofluid flow over a stretching sheet with thermal radiation, convective and slip boundary conditions. Mustafa and Khan [42] employed a fourth-fifth-order-Runge-Kutta integration scheme to obtain comprehensive solutions for magnetohydrodynamic Casson nanofluid over a non-linearly extending non-isothermal sheet, observing that both the temperature and nanoparticle volume fraction are enhanced with Casson fluid parameter. Ahmad et al. [43] examined MHD Casson nanofluid

Table 8
Comparison of skin friction and Nusselt numbers when $Re_D = 10, Pr = 7, \phi = 0, M = 0$ and $\beta \to \infty$.

s	t	γ	λ	Ec	Nr	Q_0	Pandey and Kumar [32]		Present results	
							$-f''(1)$	$-\theta'(1)$	$-f''(1)$	$-\theta'(1)$
0	1	2	2	0.3	0.1	0.1	2.7053	0.4340	2.6008	0.3149
0.1							1.9945	0.5402	1.9382	0.4592
0.2	1						1.5962	0.5889	1.5601	0.5290
0.1	0						1.8889	2.5173	1.8469	2.1894
	0.1						1.9245	1.8389	1.8782	1.5875
	1					0.1	1.9945	0.5402	1.9382	0.4592
						−2	2.0059	0.5728	1.9522	0.4979
						−0.1	1.9957	0.5436	1.9397	0.4633
						0	1.9951	0.5419	1.9389	0.4613
						0.5	1.9921	0.5333	1.9352	0.4510
						2	1.9818	0.5044	1.9227	0.4169
					0.3	−2	1.9983	0.5680	1.9450	0.4997
					0.5		1.9909	0.5623	1.9380	0.4994
					1		1.9733	0.5470	1.9214	0.4939
					2		1.9421	0.5174	1.8916	0.4765
					5		1.8762	0.4530	1.8250	0.4266
0	1	2	2	0.3	0.1	0.1	2.7053	0.4340	2.6008	0.3149

flow past a wedge with Newtonian heating. Raju and Sandeep numerically investigated Casson nanofluid flow over a rotating cone in a rotating frame filled with ferrous nanoparticles. Mehmood et al. [44] studied electromagnetohydrodynamic transport of Al2O3 nanoparticles in ethylene glycol over a convectively heated stretching cylinder.

To the best of author's apprehension nobody has discussed the effects of velocity and thermal slips on magnetohydrodyanmics (MHD) SA-Al_2O_3 and SA-Cu non-Newtonian nanofluids flow over a stretching cylinder in porous medium together with thermal radiation and chemical reaction. It is important to note here that in all the discussed articles on Casson nanofluids, most of the authors have used Newtonian liquids as base fluids, and nobody provided a specific example of non-Newtonian Casson fluid. However, in this work we have taken Sodium Alginate (SA) as an example of non-Newtonian Casson base fluid. SA has already been used by some of the authors as a non-Newtonian base fluid, see for example [45–49]. Copper (Cu) and alumina (Al_2O_3) are taken as nanoparticles and SA is taken as a base fluid. The fluid flow over a stretching cylinder in porous medium together with thermal radiation and chemical reaction effects is considered. Sodium Alginate (SA-NaAlg) is taken as non-Newtonian base fluid. Physically, this problem studies the heat transfer enhancement in a pipe like cylinder filled with SA-NaAlg non-Newtonian nanofluid containing Cu and Al_2O_3 nanoparticles. The problem is formulated in terms of nonlinear partial differential equations with auxiliary boundary conditions and then transformed into non-dimensional form by applying suitable similarity transformations. The resulting problem is solved numerically using shooting and fourth order Runge-Kutta method. A comparison between SA-Al_2O_3 and SA-Cu nanofluids is clearly shown and in limiting sense the present results are compared with published results from literature. Since nanofluids exhibited stronger vorticity and enhanced heat transfer rates, therefore, the present problem may have several applications in nanodevices of cylindrical shapes.

Problem formulation

Consider a steady laminar Casson nanofluid flow over a stretching porous pipe with radius a and two axis in vertical and horizontal direction (z, r(as shown in Fig. 1. A uniform magnetic field B_0 was applied in the radial direction we also assume the presence of thermal radiation and chemical reaction. It is supposed that temperature distant from and at the cylinder surface are constant T_1 and T_w respectively with ($T_w > T_1$). The induced magnetic field and ohmic heating are neglected.

We also consider regular fluid (Sodium Alginate) based nanofluid for two cases Sodium Alginate-Al_2O_3 and Sodium Alginate-Cu nanofluids. The main equations of mass, momentum and energy for this model are expressed as follows [44]:

$$\frac{\partial(rw)}{\partial z} + \frac{\partial(ru)}{\partial r} = 0 \tag{1}$$

$$\rho_{nf}\left(w\frac{\partial w}{\partial z} + u\frac{\partial w}{\partial r}\right) = \mu_{nf}\left(\left(1+\frac{1}{\beta}\right)\frac{\partial^2 w}{\partial z^2} + \frac{1}{r}\frac{\partial w}{\partial r} - \frac{w}{k} + \frac{g(\rho\beta)_{nf}}{\mu_{nf}}(T - T_\infty)\right) - \sigma_{nf}B_0^2 u \tag{2}$$

$$\rho_{nf}\left(w\frac{\partial w}{\partial z} + u\frac{\partial u}{\partial r}\right) = -\frac{\partial p}{\partial r} + \mu_{nf}\left(\frac{\partial^2 u}{\partial r^2} + \frac{1}{r}\frac{\partial u}{\partial r} - \frac{u}{r^2}\right) \tag{3}$$

$$(\rho C_p)_{nf}\left(w\frac{\partial T}{\partial z} + u\frac{\partial u}{\partial r}\right) = \left[k_{nf}\left(\frac{\partial^2 T}{\partial r^2} + \frac{1}{r}\frac{\partial T}{\partial r}\right) + Q_0(T - T_\infty) - \frac{\partial q_r}{\partial r} + \mu_{nf}\left(\frac{\partial w}{\partial r}\right)^2\right] \tag{4}$$

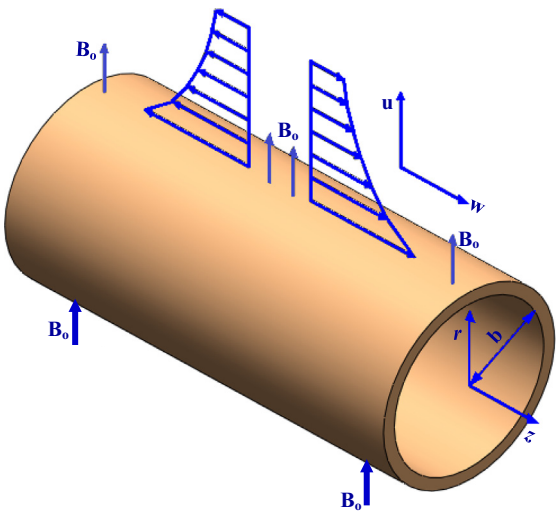

Fig. 1. Physical model.

Subject to the boundary conditions as follows:

$$u \to 0, \quad T \to T_\infty \text{ as } r \to \infty$$
$$u = U_w = 0, \quad w = W_w + L\frac{\partial w}{\partial r}, \quad T = T_w + l\frac{\partial T}{\partial r} \text{ at } r = a, \tag{5}$$

where (w; u) the component of velocity along axes (z; r) respectively. l and L are the thermal slip factor and the velocity respectively.

The subscripts ($_{sp}$; $_{bf}$) denote the nano-solid particles and regular fluid respectively.

$$\mu_{nf} = \frac{\mu_{bf}}{(1-\phi)^{2.5}} \tag{6}$$

$$\rho_{nf} = (1-\phi)\rho_{bf} + \phi\rho_{sp} \tag{7}$$

$$\alpha_{nf} = \frac{k_{nf}}{(\rho C_p)_{nf}} \tag{8}$$

$$(\rho C_p)_{nf} = (1-\phi)(\rho C_p)_{bf} + \phi(\rho C_p)_{sp} \tag{9}$$

$$\frac{k_{nf}}{k_{bf}} = \frac{k_{sp} + 2k_{bf} - 2\phi(k_{bf} - k_{sp})}{k_{sp} + 2k_{bf} + \phi(k_{bf} - k_{sp})} \tag{10}$$

$$(\rho\beta)_{nf} = (1-\phi)\rho_{bf}\beta_{bf} + \phi\rho_{sp}\beta_{sp} \tag{11}$$

where the heat capacitance $(\rho Cp)_{nf}$, the solid volume fraction φ, the thermal expansion coefficient β_{nf}, the effective dynamic viscosity μ_{nf}, the thermal diffusivity α_{nf}, the effective density ρ_{nf}, and the thermal conductivity k_{nf} of Sodium Alginate-Al_2O_3 and Sodium Alginate-Cu nanofluids

The radiative heat flux q_r, is expressed as [25] follows:

$$q_r = -\frac{16\sigma^* T_0^3}{3k^*}\frac{\partial T}{\partial r} \tag{12}$$

where (k; σ) are coefficient of mean absorption and Stefan-Boltzmann constant respectively.

The similarity transformations considered are:

$$u = -\frac{ca}{\sqrt{\eta}}f(\eta), \quad \eta = \left(\frac{r}{a}\right)^2, \quad w = 2zcf'(\eta)$$
$$\theta(\eta) = \frac{T - T_\infty}{T_w - T_\infty}, \quad \Delta T = T_w - T_\infty \tag{13}$$

Substituting Eqs. (6)–(13) into Eqs. (2) and (4), respectively, the following system is obtained:

$$\left(1+\frac{1}{\beta}\right)\eta f''' + \frac{1}{2}\left(2+\frac{1}{\beta}\right)f'' - (\lambda + \mu(1-\phi)^{2.5})f' + A_\lambda\gamma\theta + A\,\mathrm{Re}(\gamma f'' - f') = 0$$
$$\left(\frac{k_{nf}}{k_f} + \frac{4}{3}\mathrm{Nr}\right)\eta\theta'' + \left(\frac{k_{nf}}{k_f} + \frac{4}{6}\mathrm{Nr}\right)\theta' + Q_0\theta + (1-\phi)^{-2.5}\mathrm{prEc}\eta f''^2 + B\,\mathrm{Pr}\,\mathrm{Re}\,f\theta' = 0 \tag{14}$$

The suitable boundary conditions (5) change with relation to f and h

$$f'(1) = 1 + sf''(1), \quad f(1) = 0, \quad \theta(1) = 1 + t\theta'(1) \text{ at } \eta = 1$$
$$f'(\infty) \to 0, \quad \theta(\infty) \to 0 \text{ at } \eta \to \infty \tag{15}$$

where t and s are the thermal slip and the velocity slip parameters.

$$\lambda = \frac{a^2}{4k}, \quad \gamma = \frac{\beta_{bf} g a^2 \Delta T}{8zcv_{bf}}, \quad \mathrm{Ec} = \frac{4\rho_{bf}c^2z^2}{(\rho C_p)_{bf}\Delta T}, \quad \mathrm{Nr} = \left(\frac{4T_\infty^3\sigma^*}{k_{bf}k^*}\right),$$
$$\mathrm{pr} = \frac{v_{bf}}{\alpha_{bf}}, \quad Q = \frac{Q_0 a^2}{4k_{bf}}, \quad \mathrm{Re} = \frac{ca^2}{2v_{bf}} \tag{16}$$

λ the porous parameter, γ the natural convection parameter, Ec the Eckert number, Nr the radiation parameter, Pr the Prandtl number, Q is the heat generation/absorption parameter, Re_{bf} the local Reynolds number are the dimensionless parameters

A, A_1, A_2 are the constants respectively.

$$A = (1-\phi)^{2.5}\left[1 - \phi + \phi\left(\frac{\rho_{sp}}{\rho_{bf}}\right)\right] \tag{17}$$

$$A_1 = (1-\phi)^{2.5}\left[1 - \phi + \phi\left(\frac{(\rho\beta)_{sp}}{(\rho\beta)_{bf}}\right)\right] \tag{18}$$

$$A_2 = \left[1 - \phi + \phi\frac{(\rho C_p)_{sp}}{(\rho C_p)_{bf}}\right] \tag{19}$$

The skin friction coefficient and the local Nusselt number are described as follows:

$$C_f = \frac{2\mu_{nf}}{W_w^2\rho_{bf}}\left.\frac{\partial w}{\partial r}\right|_{r=a}, \quad \mathrm{Nu} = \left(\frac{-bk_{nf}}{\Delta T k_{bf}}\right)\left(\frac{\partial T}{\partial r}\right)_{r=a} \tag{20}$$

Substituting Eq. (13) in Eq. (20), the dimensionless reduced skin friction and the reduced Nusselt number becomes, respectively:

$$(z\,\mathrm{Re}/a)C_f = (\mu_{nf}/\mu_{bf})f''(1), \quad \mathrm{Nu} = -(2k_{nf}/k_{bf})\theta'(1) \tag{21}$$

Numerical method

The reduced Eqs. (14) are nonlinear and coupled, and their exact analytical solution is not possible. These equations are solved numerically using Runge-Kutta-Fehlberg method with shooting technique for different values of parameters. The effects of the emerging parameters on the dimensionless velocity, temperature, skin friction coefficient and the rate of heat transfer are investigated (Tables 1–4). The step size and convergence criteria were chosen to be 0.001 and 10^{-6} respectively. The asymptotic boundary conditions in Eq. (15) were approximated by using a value of 10 for η_{max} . This ensures that all numerical solutions approached the asymptotic values correctly (Tables 5–8).

Introducing the following variables:

$$f = x_1, f' = x_2, f'' = x_3\theta = x_4, \theta' = x_4', \theta' = x_4' \tag{22}$$

Eqs. (14) can be written as

$$\left.\begin{aligned}&\left(1+\tfrac{1}{\beta}\right)\eta x_3' + \tfrac{1}{2}\left(2+\tfrac{1}{\beta}\right)x_3 \\ &\quad -[\lambda + \mu(1-\phi)^{2.5}]x_2 + A\lambda\gamma x_4 + A\,\mathrm{Re}(\gamma x_3 - x_2) = 0 \\ &\left(\tfrac{k_{nf}}{k_f} + \tfrac{4}{3}\mathrm{Nr}\right)\eta x_4'' + \left(\tfrac{k_{nf}}{k_f} + \tfrac{4}{6}\mathrm{Nr}\right)x_4' \\ &\quad + Q_0 x_4 + (1-\phi)^{-2.5}\mathrm{PrEc}\eta x_3^2 + B\,\mathrm{Pr}\,\mathrm{Re}\,x_1 x_4' = 0\end{aligned}\right\} \tag{23}$$

with boundary conditions

$$x_2(1) = 1 + s\gamma_1, \quad x_1(1) = 0, \quad x_4(1) = 1 + tx_4'(1),$$
$$x_3(1) = \gamma_1, \quad x_4(1) = \gamma_2 \text{ at } \eta = 1$$
$$x_2(\infty) \to 0, \quad x_4(\infty) \to 0 \text{ at } \eta \to \infty \tag{24}$$

where γ_1 and γ_2 are the unknown initial conditions and can be determined using the shooting method.

Results and discussion

A Casson nanofluid steady flow over a stretching porous cylinder with natural convection and slip boundary conditions in the presence of magnetic fields, heat source/sink, thermal radiation and viscous dissipation has been investigated numerically by

means of shooting scheme based Runge-Kutta-Fehlberg-integration algorithm. In this study Sodium Alginate-based nanofluids with nanoparticles of Cu and Al_2O_3 are used.

The effects of slip velocity and solid volume fraction of Cu and Al_2O_3 nanoparticles on the dimensionless velocity are depicted in Fig. 2(a) and (b) respectively for the other values are set constantly of $N_r = Q_0 = 0.1$; $\gamma = \lambda = 2$; $E_c = 0.3$; $P_r = 6$; $Re = 10$. It is perceived that, the dimensionless velocity is the highest for both Cu and Al_2O_3 nanoparticles at the surface of the cylinder and progressively decreases to zero as it moves away from the surface of the cylinder. It is further observed that, the dimensionless velocity increase with solid volume fraction while it decreases with slip velocity for both Cu and Al_2O_3 nanoparticles. We realize that, in the absence of slip velocity (s = 0) and at the surface of the cylinder the dimensionless velocity has the highest value and loss 40% when s = 0.5. Therefore, the slip velocity parameter is expected to alter the hydrodynamic boundary layer significantly. This can be attributed to the facts that for no slip condition the fluid velocity near the stretching cylinder will not be equal to the stretching cylinder velocity. This signifies that the boundary layer thickness decreases with the slip parameter. Furthermore, it is found that the dimensionless velocity for both Cu and Al_2O_3 nanoparticles are seen to be enhanced in magnitude with increasing volume fraction values. Therefore, the boundary layer thickness increases which in turn amplify the hydrodynamic resistance. It is remarked that for regular fluids ($\phi = 0$) the velocity profile has the lowest value compared to other case with solid volume fraction. It is clear that the behavior of velocity profiles for both Cu and Al_2O_3 nanoparticles are the same. However, dimensionless velocity of Sodium Alginate-Cu is higher than Sodium Alginate-Al_2O_3, in case no slip flow and $\eta = 3$ the dimensionless velocity of Sodium Alginate-Cu is 0.2 whereas for Sodium Alginate-Al_2O_3 the dimensionless velocity is 0.1. This can be elucidated by the fact that, the density of Cu is around double of Al_2O_3 nanoparticles.

Fig. 3(a) and (b) present the effects of magnetic field and Casson fluid parameter on dimensionless velocity for Sodium Alginate-Al_2O_3 and Sodium Alginate-Cu nanofluids respectively. It is observed that the dimensionless velocity increase with casson fluid parameter, while it decrease with magnetic field parameter for both case of Sodium Alginate-Al_2O_3 and Sodium Alginate-Cu nanofluids, In an unexpected and perplexing results revealed by Fig. 3 the velocity profile increase with casson fluid parameter β this can be attributed to the fact that the yield stress substantially decrease and consequently the velocity increase, accordingly boundary layer thickness increase with casson fluid parameter. The dimensionless velocity reduces with increasing in magnetic field parameter promoting to a lessening in the velocity boundary layer thickness. It is worthwhile to note that in the absence of mag-

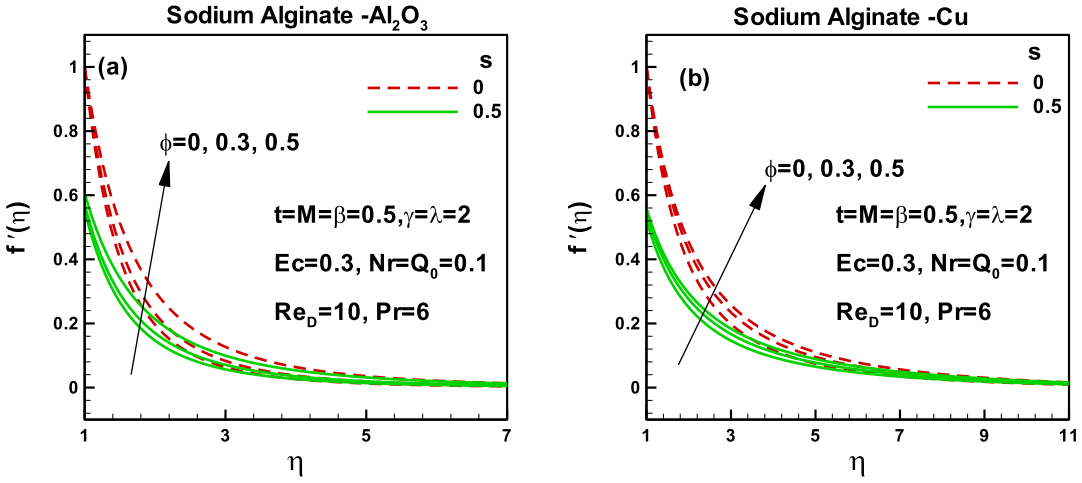

Fig. 2. Effects of slip velocity and solid volume fraction of nanoparticles on dimensionless velocity for (a) Sodium Alginate-Al_2O_3 and (b) Sodium Alginate-Cu nanofluids.

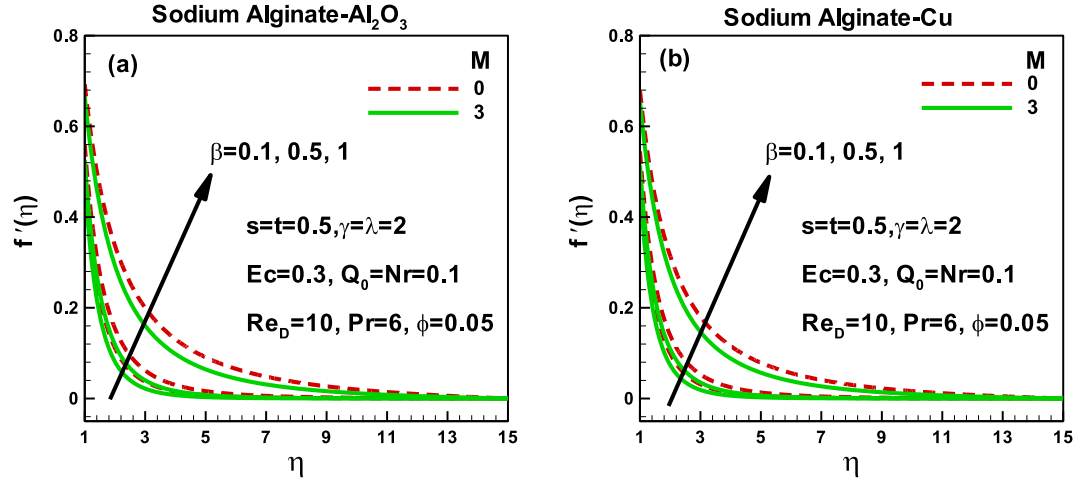

Fig. 3. Effects of magnetic field and Casson fluid parameter on dimensionless velocity for (a) Sodium Alginate-Al_2O_3 and (b) Sodium Alginate-Cu nanofluids.

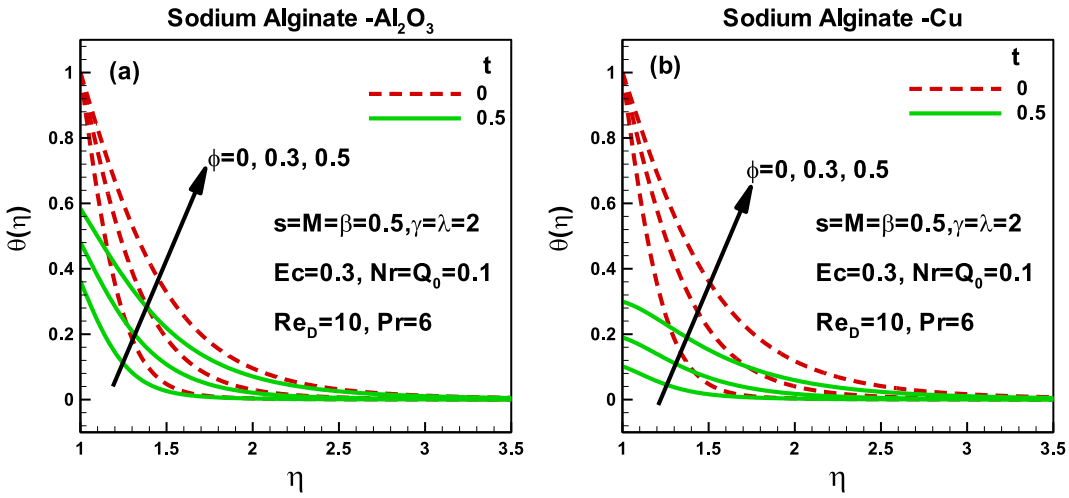

Fig. 4. Effects of thermal slip and solid volume fraction of nanoparticles on dimensionless temperature for (a) Sodium Alginate-Al_2O_3 and (b) Sodium Alginate-Cu nanofluids.

netic field and for higher value of Casson fluid parameters, the dimensionless velocity for both Sodium Alginate-Al_2O_3 and Sodium Alginate-Cu nanofluids has the highest values and decreases feebly with the applied transverse magnetic field, the physical reason behind this is that magnetic field promote Lorentz force which in turn opposes the flow and decrease the dimensionless velocity.

The effects of thermal slip and solid volume fraction of nanoparticles on dimensionless temperature for Sodium Alginate-Al_2O_3 and Sodium Alginate-Cu nanofluids are exposed in Fig. 4 (a) and (b) respectively. As expected, the dimensionless temperature is higher at the surface of the cylinder then decrease along the streamwise direction until 0 for both cases of Sodium Alginate-Al_2O_3 and Sodium Alginate-Cu nanofluids. We realize that temperature profile increase as solid volume fraction of nanoparticles increase, whereas, it decrease meaningfully with thermal slip parameter. The physical reason behind this is that the thermal slip parameter reduces heat transfer rate which in turn the dimensionless temperature lessens. It should be pointed out that the concentration affects the Brownian movement which in turn enhances the thermal conductivity of the nanofluid and heat transfer rate. Consequently, the dimensionless temperature parameter is expected to increase with solid volume fraction of nanoparticles. It is remarked that in the absence of thermal slip effect the dimensionless temperature has the same behavior for both Sodium Alginate-Al_2O_3 and Sodium Alginate-Cu nanofluids, and with slip thermal Sodium Alginate-Cu nanofluids reveal lesser dimensionless temperature inside thermal boundary layer and hence smaller thermal boundary layer thickness. For regular fluids (ϕ=0), the surface dimensionless temperature in case of Cu nanoparticles is 30% compared to Al_2O_3 nanoparticles, this can be explain by the fact that the thermal diffusivity of Cu nanoparticles higher than Al_2O_3 nanoparticles, and then reduce the temperature gradients.

Fig. 5(a) and (b) have been drawn to illustrate the effect of radiation and heat generated parameters on dimensionless temperature for Sodium Alginate-Al_2O_3 and Sodium Alginate-Cu nanofluids respectively. It can be seen that dimensionless temperature for both Sodium Alginate-Al_2O_3 and Sodium Alginate-Cu nanofluids increases with both radiation *Nr* and heat generated parameter Q_0, which signifies that thermal boundary layer thickness rises along with radiation and heat generation, this can be attributed to the substantial penetration of the heat into the fluid and thus both temperature and thermal boundary layer thickness increase. Accordingly, higher value of thermal radiation indicates higher surface heat flux. Therefore, the temperature profile grows dramatically. Moreover, as observed the temperature profile increase as heat generation parameter increase, this effect occur

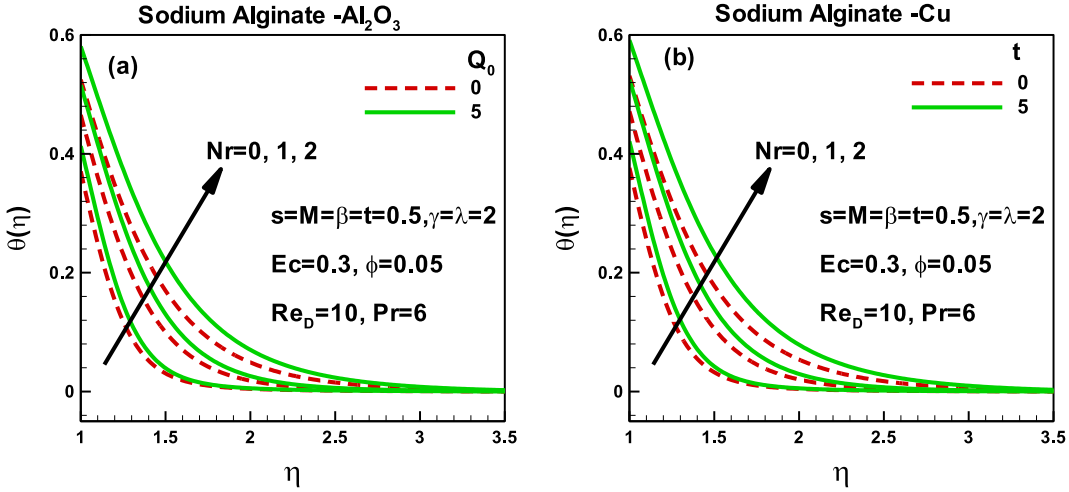

Fig. 5. Effects of radiation and heat generated parameters on dimensionless temperature for (a) Sodium Alginate-Al_2O_3 and (b) Sodium Alginate-Cu nanofluids.

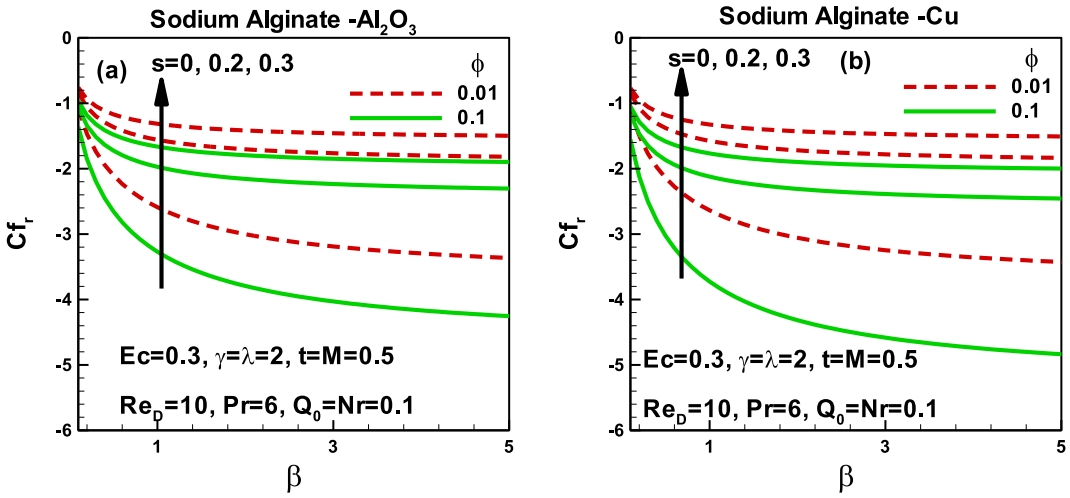

Fig. 6. Variation of skin friction with slip velocity, Casson fluid parameter and solid volume fraction of nanoparticles for (a) Sodium Alginate-Al_2O_3 and (b) Sodium Alginate-Cu nanofluids.

due to the fact that heat generation represent a sort of heat sink and so affect directly the dimensionless temperature.

The effects of slip velocity, Casson fluid parameter and solid volume fraction of nanoparticles on skin friction are described in Fig. 6 (a) for Cu-Sodium Alginate and in Fig. 6(b) for Al_2O_3-Sodium Alginate. It is perceived that for both case with Cu nanoparticles and Al_2O_3 nanoparticles the skin friction increases with slip velocity, while it decreases with Casson fluid parameter and solid volume fraction of nanoparticles. This is caused by the effect of dimensionless velocity inside the boundary layer and accordingly affects the boundary layer thickness, as proved by Figs. 2 and 3.

It can be realized that, the skin friction is maximum for Casson fluid parameter β very small and declines significantly in case of non-slip velocity and higher solid volume fraction of nanoparticles. However for higher slip velocity and lower solid volume fraction of nanoparticle the skin friction decrease meaningless with Casson fluid parameter. It is worthwhile to note that for a regular fluid φ = 0, the skin friction is less important and rises with the solid volume fraction of nanoparticles in both cases of Cu and Al_2O_3 nanoparticles. It is clear that the behavior of skin friction for both Cu and Al_2O_3 nanoparticles are the same.

Fig. 7(a) and (b) display the effects of magnetic field, Reynolds number and porous parameter on skin friction for Sodium Alginate-Al_2O_3 and Sodium Alginate-Cu nanofluids respectively. It is important to note that the skin friction decreases continually and meaningfully with porous parameter, magnetic field and Reynolds number for both case with Cu nanoparticles and Al_2O_3 nanoparticles. It is clear that in the absence of a magnetic field, the skin friction is found to be higher and decreases with an increase in the magnetic field. This can be attributed to the substantial increase on Lorentz force which transverse and pushes the flow from the surface which in turn lessen the friction at the surface of the cylinder. The lessening of skin friction with porous parameter can be can be attributed to the increasing of the fluid velocity which mains to the velocity boundary layer enlarging. It is well known that increasing Reynold number leads to reducing viscous force compared to inertial force and it can be interpreted on this fact that the reducing viscous force will diminish skin friction. It is worthwhile to note that the behavior of skin friction for both Cu and Al_2O_3 nanoparticles are the same.

The variation of Nusselt number with thermal slip, Casson fluid parameter and solid volume fraction of nanoparticles for Sodium Alginate-Al_2O_3 and Sodium Alginate-Cu nanofluids are exposed in Fig. 8(a) and (b) respectively. It is indicates that Nusselt number decreases with Casson fluid parameter, thermal slip and solid volume fraction of nanoparticles for both Cu and Al_2O_3 nanoparticles.

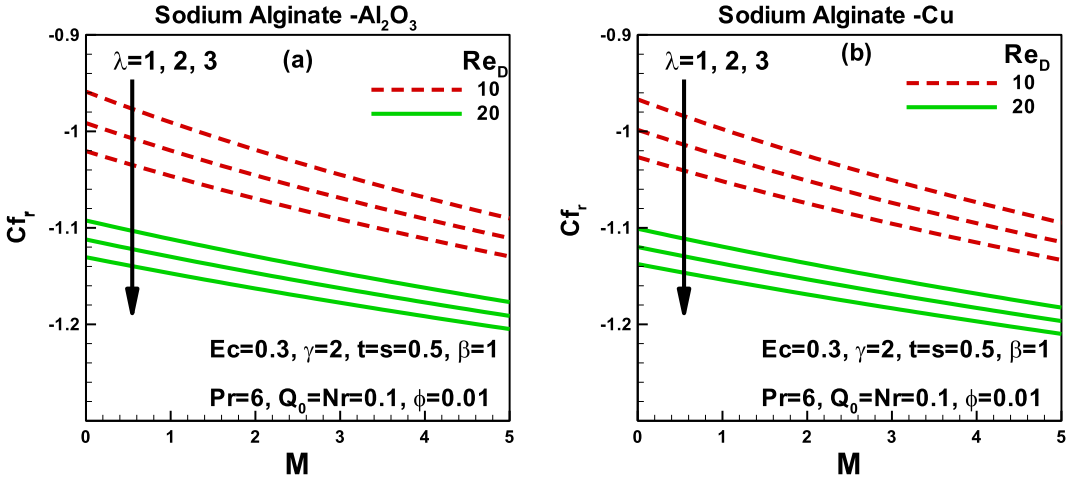

Fig. 7. Variation of skin friction with magnetic field, Reynolds number and porous parameter for (a) Sodium Alginate-Al_2O_3 and (b) Sodium Alginate-Cu nanofluids.

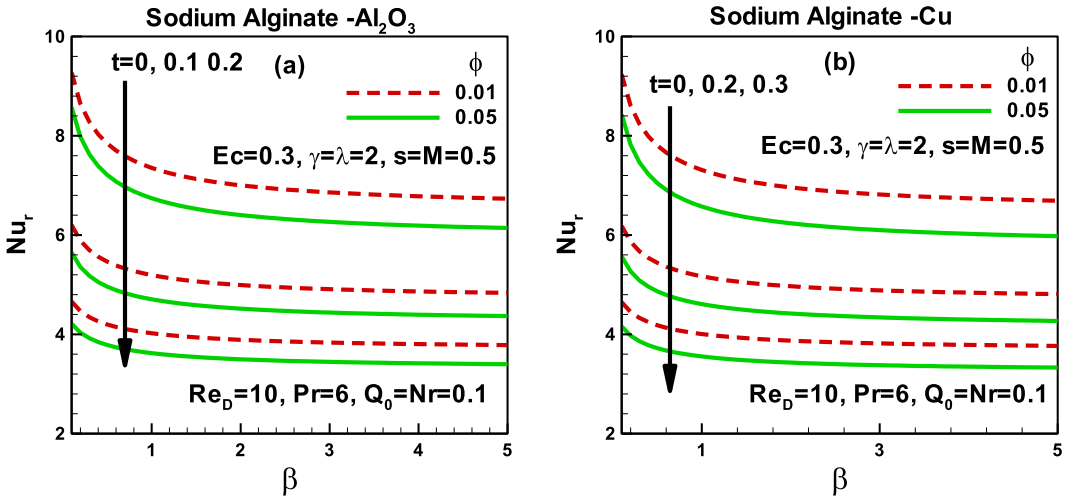

Fig. 8. Variation of Nusselt number with thermal slip, Casson fluid parameter and solid volume fraction of nanoparticles for (a) Sodium Alginate-Al_2O_3 and (b) Sodium Alginate-Cu nanofluids.

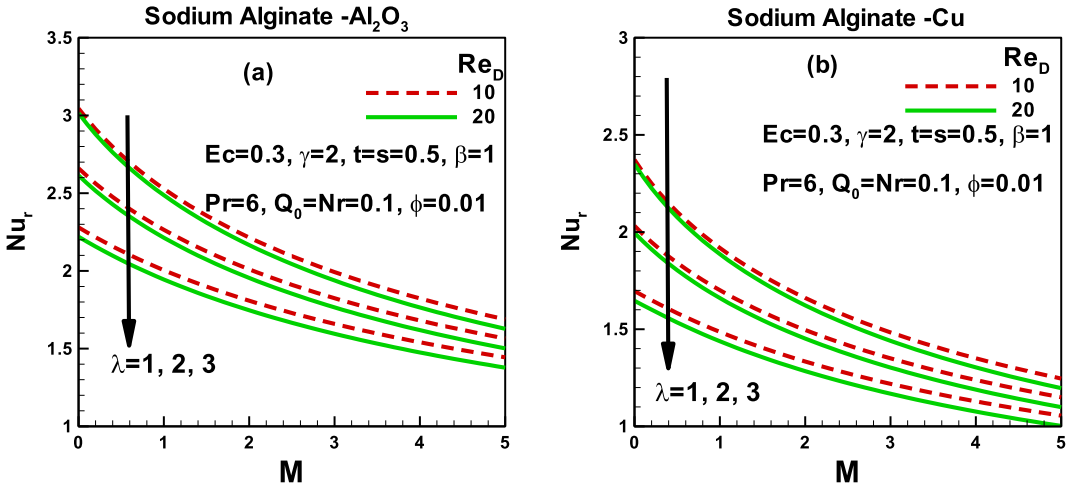

Fig. 9. Variation of Nusselt number with magnetic field, Reynolds number and porous parameter for (a) Sodium Alginate-Al_2O_3 and (b) Sodium Alginate-Cu nanofluids.

This signifies that Casson fluid parameter, thermal slip and solid volume fraction of nanoparticles enhance severely conduction compared to convection heat transfer. The Nusselt numbers are found to be higher for Casson fluid parameter β very small and declines significantly until $\beta = 2$ when Nusselt numbers remain nearly constant, this is due to the fact that the increasing of thermal boundary layer with Casson fluid parameter β will enhances the thermal resistance. No appreciable alteration on the Nusselt number could be observed whether changing nanoparticles (Cu or Al_2O_3), this is due to neglected variation of skin friction with used nanoparticles. It is clear that the Nusselt number depends upon the thermal slip parameter, since the skin friction is decreased extremely with it as revealed by Fig. 6.

Fig. 9(a) and (b) exhibit the effect of magnetic field, Reynolds number and porous parameter on Nusselt number for Sodium Alginate-Al_2O_3 and Sodium Alginate-Cu nanofluids respectively. It can be seen that Nusselt number decrease with porous parameter, magnetic field and Reynolds number, this effect is graphically obvious and approved by previous Fig. 7. However, this Fig. 9 shows that Nusselt numbers which represent the ratio of convection to conduction heat transfer are the highest in case of Al_2O_3 than Cu nanoparticles since the thermal conductivity of Cu is higher than Al_2O_3 nanoparticles and therefore Nusselt numbers will be smaller for Sodium Alginate-Cu nanofluids. It should be pointed out that Reynolds number, porous parameter and magnetic field enhances the conduction compared to convection heat transfer. Furthermore, in the absence of magnetic field it is found that Nusselt number is highest for both cases Sodium Alginate-Al_2O_3 and Sodium Alginate-Cu nanofluids and it decreases when a magnetic field is applied.

Conclusions

The effect of Multiple Slips on steady Casson nanofluid over a stretching porous cylinder and heat transfer of Sodium Alginate-Al_2O_3 and Sodium Alginate-Cu nanofluids in the presence of thermal radiation, magnetic field and chemical radiation has been investigated numerically by using Keller box and Newton-Raphson methods. The study reveals major results are as follows:

- The dimensionless velocity increase with solid volume fraction while it decreases with slip velocity for both Cu and Al_2O_3 nanoparticles. Moreover, it has the highest value at the surface of the cylinder and progressively decreases until zero along streamwise direction.

- The dimensionless velocity increase with casson fluid parameter, while it decrease with magnetic field parameter for both case of Sodium Alginate-Al_2O_3 and Sodium Alginate-Cu nanofluids. In the absence of magnetic field and for higher value of Casson fluid parameters, the dimensionless velocity has the highest values and decreases weakly with the applied transverse magnetic field.
- Temperature profile increase with thermal radiation *Nr*, heat generation parameter Q_0 and solid volume fraction of nanoparticles, although, it decrease significantly with thermal slip parameter.
- Dimensionless temperature is higher at the surface of the cylinder then decrease along the streamwise direction until 0 for both cases of Sodium Alginate-Al_2O_3 and Sodium Alginate-Cu nanofluids.
- Casson fluid parameter, solid volume fraction of nanoparticles, magnetic field, Reynolds number and porous parameter reduce meaningfully the Skin friction. While, it increases as enhanced in slip velocity. For a regular fluid $\varphi = 0$, the skin friction is less important.
- Nusselt number decreases with Casson fluid parameter, thermal slip, porous parameter, magnetic field, Reynolds number and solid volume fraction for both Cu and Al_2O_3 nanoparticles.
- Nusselt numbers are the highest in case of Al_2O_3 than Cu nanoparticles due to the fact that thermal conductivity of Cu is higher than Al_2O_3 nanoparticles.

Appendix A. Supplementary data

Supplementary data associated with this article can be found, in the online version, at https://doi.org/10.1016/j.rinp.2017.12.013.

References

[1] Wang CY. Fluid flow due to a stretching cylinder. Phys Fluids 1988;31 (3):466–8.
[2] Ishak A, Nazar R, Pop I. Uniform suction/blowing effect on flow and heat transfer due to a stretching cylinder. Appl Math Model 2008;32(10):2059–66.
[3] Khan I, Farhad A, Samiulhaq, Sharidan S. Exact solutions for unsteady MHD oscillatory flow of a Maxwell fluid in a porous medium. Z Naturfors Sect A-J Phys Sci 2013:1–11.
[4] Abdulhameed M, Khan I, Shardian S, Vieru D. Exact solutions for unsteady flow of a second grade fluid generated by an oscillating wall with transpiration. Appl Math Mech 2014;35(7):821–30.
[5] Mahmoud MAA. Slip velocity effect on a non-Newtonian power-law fluid over a moving permeable surface with heat generation. Math Comput Modell 2011;54(5–6):1228–37.
[6] Hayat Tasawar, Qayyum Sajid, Alsaedi Ahmed, Shafiq Anum. Inclined magnetic field and heat source/sink aspects in flow of nanofluid with nonlinear thermal radiation. Int J Heat Mass Transfer 2016;103:99–107.
[7] Qayyum Sajid, Hayat Tasawar, Alsaedi Ahmed. Chemical reaction and heat generation/absorption aspects in MHD nonlinear convective flow of third grade nanofluid over a nonlinear stretching sheet with variable thickness. Results Phys 2017;7:2752–61.
[8] Waqas Muhammad, Farooq Muhammad, Khan Muhammad Ijaz, Alsaedi Ahmed, Hayat Tasawar, Yasmeen Tabassum. Magnetohydrodynamic (MHD) mixed convection flow of micropolar liquid due to nonlinear stretched sheet with convective condition. Int J Heat Mass Transfer 2016;102:766–72.
[9] Qayyum Sajid, Hayat Tasawar, Alsaedi Ahmed, Ahmad Bashir. Magnetohydrodynamic (MHD) nonlinear convective flow of Jeffrey nanofluid over a nonlinear stretching surface with variable thickness and chemical reaction. Int J Mech Sci 2017;134:306–14.
[10] Hayat Tasawar, Qayyum Sajid, Alsaedi Ahmed, Ahmad Bashir. Magnetohydrodynamic (MHD) nonlinear convective flow of Walters-B nanofluid over a nonlinear stretching sheet with variable thickness. Int J Heat Mass Transfer 2017;110:506–14.
[11] Qayyum Sajid, Hayat Tasawar, Alsaedi Ahmed. Bashir Ahmad", MHD nonlinear convective flow of thixotropic nanofluid with chemical reaction and Newtonian heat and mass conditions". Results Phys 2017;7:2124–33.
[12] Hayat Tasawar, Qayyum Sajid, Alsaedi Ahmed, Asghar Saleem. Radiation effects on the mixed convection flow induced by an inclined stretching cylinder with non-uniform heat source/sink. PLoS One 2017;12(4).
[13] Casson N. A flow equation for the pigment oil suspensions of the printing ink type, in rheology of disperse systems, 84-102. New York: Pergamon; 1959.
[14] Bhattacharyya K. Boundary layer stagnation-point flow of Casson fluid and heat transfer towards a shrinking/stretching sheet. Frontiers in Heat and Mass Transfer (FHMT), vol. 4, Article ID 023003; 2013.
[15] Bhattacharyya K, Hayat T, Alsaedi A. Exact solution for boundary layer flow of Casson fluid over a permeable stretching/shrinking sheet. Z Angew Math Mech 2013;10:1–7.
[16] Bhattacharyya K, Hayat T, Alsaedi A. Analytic solution for magnetohydrodynamic boundary layer flow of Casson fluid over a stretching/shrinking sheet with wall mass transfer. Chin Phys B 2013;22:024702.
[17] Mukhopadhyay S, De Rajan P, Bhattacharyya K. Casson fluid flow over an unsteady stretching surface. Ain Shams Eng J 2013;4:933–8.
[18] Pramanik S. Casson fluid flow and heat transfer past an exponentially porous stretching surface in presence of thermal radiation. Ain Shams Eng J 2014;5:205–12.
[19] Benazir AJ, Sivaraj R, Rashidi MM. Comparison between Casson fluid flow in the presence of heat and mass transfer from a vertical cone and flat plate. J Heat Transfer 2016;138(11):112005.
[20] Animasaun IL. Casson fluid flow with variable viscosity and thermal conductivity along exponentially stretching sheet embedded in a thermally stratified medium with exponentially heat generation. Journal of Heat and Mass Transfer Research 2015;2(2):63–78.
[21] Raju CSK, Sandeep N. MHD slip flow of a dissipative Casson fluid over a moving geometry with heat source/sink: a numerical study. Acta Astronaut 2016.
[22] Kirubhashankar CK, Ganesh S. Unsteady MHD flow of a Casson fluid in a parallel plate channel with heat and mass transfer of chemical reaction. Indian J Res 2014;3:101–5.
[23] Hayat T, Shehzad SA, Alsaedi A, Alhothuali MS. Mixed convection stagnation point flow of Casson fluid with convective boundary conditions. Chin Phys Lett 2012;29:114704.
[24] Mahanta G, Shaw S. 3D Casson fluid flow past a porous linearly stretching sheet with convective boundary condition. Alex Eng J 2015;54:653–9.
[25] Abou-zeid Mohamed. Effects of thermal-diffusion and viscous dissipation on peristaltic flow of micropolar non-Newtonian nanofluid: application of homotopy perturbation method. Results Phys 2016;6:481–95.
[26] El-dabe Nabil TM, Abou-zeid Mohamed Y, Younis Yasmeen M. Magnetohydrodynamic peristaltic flow of jeffry nanofluid with heat transfer through a porous medium in a vertical tube. Appl. Math Inf Sci 2017;11 (4):1097–103.
[27] Mohamed Abou-zeid. Homotopy Perturbation Method to Gliding Motion of Bacteria on a Layer of Power-Law Nanoslime with Heat Transfer. 2015;12:3605–14(10).
[28] Abou-zeid Mohamed. Homotopy perturbation method for mhd non-newtonian nanofluid flow through a porous medium in eccentric annuli with peristalsis. Therm Sci 2017;21(5):2069–80.
[29] Abou-zeid Mohamed, Mohamed Mona AA. Homotopy perturbation method for creeping flow of Non-Newtonian power-law nanofluid in a nonuniform inclined channel with peristalsis. Zeitschrift für Naturforschung A 2017;72. ISSN 1865-7109.
[30] Choi S. Development and applications of non-Newtonian flows. ASME 1995;66:99–105.
[31] Ahmed SE, Hussein AK, Mohammed HA, Sivasankaran S. Boundary layer flow and heat transfer due to permeable stretching tube in the presence of heat source/sink utilizing nanofluids. Appl Math Comput 2014;238:149–62.
[32] Pandey AK, Kumar M. Natural convection and thermal radiation influence on nanofluid flow over a stretching cylinder in a porous medium with viscous dissipation. Alex Eng J 2017;56:55–62.
[33] Ashorynejad HR, Sheikholeslami M, Pop I, Ganji DD. Nanofluid flow and heat transfer due to a stretching cylinder in the presence of magnetic field. Heat Mass Transfer 2013;49:427–36.
[34] Buongiomo J. Convective transport in nanofluids. ASME Trans J Heat Transfer 2006;128:240–50.
[35] Nield DA, Kuznetsov AV. The Cheng-Minkowycz problem for natural convective boundary layer flow in a porous medium saturated by a nanofluid. Int J Heat Mass Transfer 2009;52:5792–5.
[36] Haq R, Nadeem S, Khan ZH, Okedayo Toyin Gideon. Convective heat transfer and MHD effects on Casson nanofluid flow over a shrinking sheet. Cent Eur J Phys 2014;12:862–71.
[37] Nadeem S, Haq R, Akbar NS. MHD three-dimensional boundary layer flow of Casson nanofluid past a linearly stretching sheet with convective boundary condition. IEEE Trans Nanotechnol 2014;13:109–15.
[38] Abolbashari MH, Freidoonimehr N, Nazari F, Rashidi MM. Analytical modeling of entropy generation for Casson nanofluid flow induced by a stretching surface. Adv Powder Technol 2015;26:542–52.
[39] Hussain T, Shehzad S, Alsaedi T Hayat, Ramzan M. Flow of Casson nanofluid with viscous dissipation and convective conditions: A mathematical model. J Cent South Univ 2015;22:1132–40.
[40] Sulochana C, Ashwinkumar GP, Sandeep N. Similarity solution of 3D Casson nanofluid flow over a stretching sheet with convective boundary conditions. J Niger Math Soc 2016;35:128–41.
[41] Oyelakin IS, Mondal S, Sibanda P. Unsteady Casson nanofluid flow over a stretching sheet with thermal radiation, convective and slip boundary conditions. Alex Eng J 2016;55:1025–35.

[42] Mustafa M, Khan JA. Model for flow of Casson nanofluid past a non-linearly stretching sheet considering magnetic field effects. AIP Adv 2015;5:077148.
[43] Ahmad K, Hanouf Z, Ishak A. MHD Casson nanofluid flow past a wedge with Newtonian heating. A Eur Phys J Plus 2017;132:87. https://doi.org/10.1140/epjp/i2017-11356-5.
[44] Mehmood OU, Maskeen MM, Zeeshan A. Electromagnetohydrodynamic transport of Al_2O_3 nanoparticles in ethylene glycol over a convectively heated stretching cylinder. Adv Mech Eng 2017;9(11):1–8. https://doi.org/10.1177/1687814017735282.
[45] Raju CSK, Sandeep N. Unsteady Casson nanofluid flow over a rotating cone in a rotating frame filled with ferrous nanoparticles: a numerical study. J Magn Magn Mater 2017;421(1):216–24.
[46] Liakos I, Rizzello L, Scurr DJ, Pompa PP, Bayer IS, Athanassiou A. All natural composite wound dressing films of essential oils encapsulated in sodium alginate with antimicrobial properties. Int J Pharm 2014;463:137–45.
[47] Hatami M, Ganji DD. Heat transfer and flow analysis for SA-TiO_2 non-Newtonian nanofluid passing through the porous media between two coaxial cylinders. J Mol Liq 2013;188:155–61.
[48] Hatami M, Ganji DD. Natural convection of sodium alginate (SA) non-Newtonian nanofluid flow between two vertical flat plates by analytical and numerical methods. Case Stud Therm Eng 2014;2:14–22.
[49] Pawar SS, Sunnapwar VK. Experimental studies on heat transfer to Newtonian and non-Newtonian fluids in helical coils with laminar and turbulent flow. Exp Therm Fluid Sci 2013;44:792–804.